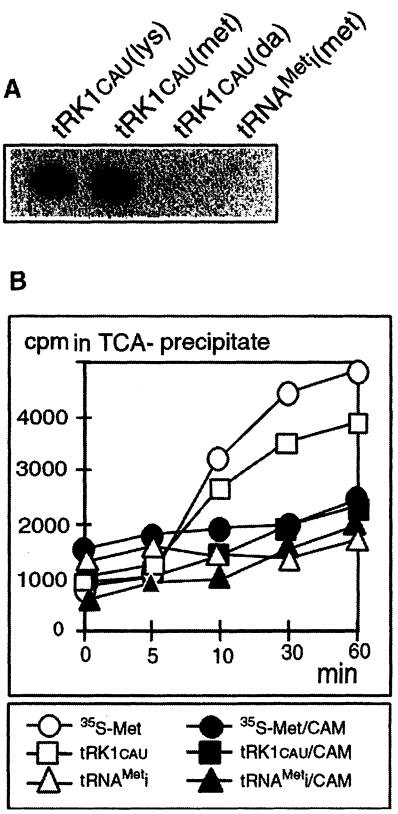

Fig. 4. Imported $tRK1_{CAU}$ is active in human mitochondrial translation. (**A**) In vitro import of labeled tRNAs into isolated HepG2 mitochondria. (**B**) Kinetics of incorporation of [^{35}S]Met into mitochondrial polypeptides. $tRK1_{CAU}$ and $tRNA^{Met}i$ were aminoacylated by the yeast MetRS. Intraorganelle protein synthesis was as in (*29*). Free [^{35}S]Met was used as a control. Equal molar amounts of [^{35}S]Met were used in each case. "/CAM" indicates addition of chloramphenicol at 100 μg/ml.

and found that tRNA import selectivity is similar in human and yeast mitochondria. As expected, $tRK1_{CAU}$ was efficiently imported in its methionylated form (Fig. 4A). This finding was exploited to test whether $tRK1_{CAU}$ is active in human mitochondrial translation. We observed chloramphenicol-sensitive incorporation of [^{35}S]Met into mitochondrial protein after import of [^{35}S]Met-$tRK1_{CAU}$ (Fig. 4B), and the labeled polypeptides were shown to contain antigenic determinants for human Cox1p. Therefore, the imported yeast cytosolic tRNA is functional on the human mitochondrial translation apparatus.

These results suggest the possibility of developing a tRNA mitochondrial import system in human cells. Such a system could be useful for either suppressing nonsense mutations in protein-coding genes or to replace nonfunctional mutant tRNAs.

References and Notes

1. A. Schneider, *Trends Cell Biol.* **4**, 282 (1994).
2. I. A. Tarassov, N. S. Entelis, R. P. Martin, in *Mitochondrial Diseases, Models and Methods*, P. Lestienne, Ed. (Springer-Verlag, Berlin, 1999), pp. 303–316.
3. R. P. Martin, J.-M. Schneller, A. Stahl, G. Dirheimer, *Biochemistry* **18**, 4600 (1979).
4. I. A. Tarassov, N. S. Entelis, R. P. Martin, *J. Mol. Biol.* **245**, 315 (1995).
5. ———, *EMBO J.* **14**, 3461 (1995).
6. N. S. Entelis, I. A. Krashenninikov, R. P. Martin, I. A. Tarassov, *FEBS Lett.* **384**, 38 (1996).
7. N. S. Entelis, S. Kieffer, O. A. Kolesnikova, R. P. Martin, I. A. Tarassov, *Proc. Natl. Acad. Sci. U.S.A.* **95**, 2838 (1998).
8. H. A. Kazakova, N. S. Entelis, R. P. Martin, I. A. Tarassov, *FEBS Lett.* **442**, 193 (1999).
9. A. Dietrich, L. Maréchal-Drouard, V. Carneiro, A. Cosset, I. Small, *Plant J.* **10**, 913 (1996).
10. A. Mireau *et al.*, *J. Biol. Chem.* **275**, 13291 (2000).
11. S. Adhya, T. Ghosh, A. Das, S. K. Bera, S. Mahapatra, *J. Biol. Chem.* **272**, 21396 (1997).
12. C. E. Nabholz, E. K. Horn, A. Schneider, *Mol. Biol. Cell* **10**, 2547 (1999).
13. A. E. Yermovsky-Krammerer and S. Hajduk, *Mol. Cell. Biol.* **19**, 6253 (1999).
14. R. Aphasizhev, B. Senger, F. Fasiolo, *RNA* **3**, 489 (1997).
15. E. McKee and R. Poyton, *J. Biol. Chem.* **259**, 9320 (1984).
16. The absence of incorporation of [^{35}S]Met into proteins after incubation of mitochondria with $tRNA^{Met}i$, which is not imported, indicates that deacylation and reuse of the free-labeled amino acid by mtMetRS does not occur.
17. To construct the HM4 strain, an *amber* codon was introduced at alanine codon 114 of the *COX2* gene by oligonucleotide-directed mutagenesis of pJM2 (*18*). The mutagenized plasmid was introduced into the mitochondria of MCC123ρ^0 cells by high-velocity microprojectile bombardment (*19*). Transformed cells harboring the mutant plasmid were selected by screening for marker-rescue of the *cox2-103* allele after mating to strain HMD3. The $cox2^{amber}$ mutation was then integrated into mtDNA by cytoduction of the ρ^- mitochondria into strain NB40-16B. Recombinant ρ^+ progeny were identified by their ability to marker-rescue the *cox2-103* mutation after crossing to HMD13. The presence of the $cox2\text{-}114^{amber}$ mutation in the ρ^+ mtDNA was verified by sequencing the relevant region of the *COX2* gene. Genotype of HM4 is *MATα leu2-3,112 lys2 ura3-52 arg8::hisG* [ρ^+ $cox2\text{-}114^{amber}$].
18. J. Mulero and T. D. Fox, *Mol. Biol. Cell* **4**, 1327 (1993).
19. G. Wiesenberger, M. Costanzo, T. D. Fox, *Mol. Cell. Biol.* **15**, 3291 (1995).
20. Y. Hou and P. Schimmel, *Nature* **333**, 140 (1988).
21. U. Varshney, C. Lee, U. RajBhandary, *J. Biol. Chem.* **266**, 24712 (1991).
22. D. C. Wallace, *Science* **283**, 1482 (1999).
23. P. Magalhaes, A. Andreu, E. Schon, *Mol. Biol. Cell* **9**, 2375 (1998).
24. C. Doersen, C. Guerrier-Takada, S. Altman, G. Attardi, *J. Biol. Chem.* **260**, 5942 (1985).
25. K. Li *et al.*, *J. Cell Biol.* **124**, 871 (1994).
26. G. Schatz and B. Dobberstein, *Science* **271**, 1519 (1996).
27. G. Gaines and G. Attardi, *Mol. Cell. Biol.* **4**, 1605 (1984).
28. HmIDPs were prepared as ScIDPs (*3*), except for cell lysis conditions. The cell culture flasks were washed with phosphate-buffered saline (PBS) and incubated for 5 min at 37°C in PBS containing 1 mM EDTA. The cells were collected, washed with PBS without EDTA, resuspended in HKM [10 mM Hepes-KOH (pH 6.5), 50 mM KCl, 2 mM $MgCl_2$] with 10% glycerol in the presence of a cocktail of protease inhibitors, and disrupted by sonication. After removal of nucleic acids by polyethylenimine treatment, proteins were collected from the supernatant by ammonium sulfate precipitation (70%) and dialyzed against HKM with 50% glycerol.
29. D. Beattie and K. Sen, in *Mitochondria: A Practical Approach*, V. Darley-Usmar, D. Rickwood, M. Wilson, Eds. (IRL Press, Oxford, 1987), pp. 283–310.

30. We thank F. Fasiolo, G. Keith, M. Mirande (CNRS, France), N. Pfanner (Freiburg University, Germany), and A. Tzagoloff (Columbia University, USA) for providing strains, enzymes, antibodies, and tRNAs. We also thank members of the laboratory of R. N. Lightowlers (Newcastle University, UK) and A. Schneider (Fribourg University, Switzerland) for critical discussions of the results. This work was supported by CNRS, Université Louis Pasteur (ULP), Moscow University, Association Française contre les Myopathies (AFM), International Association for Promotion of Cooperation with Scientists from the New Independent States of the Former Soviet Union (INTAS) (grant 96-1515), Human Frontier Science Program (HFSP) (grant RG0349/1999-M), and NIH (grant GM29362). O.K. was supported by a Federation of European Biochemical Societies fellowship; N.E. was supported by ULP, CNRS, and HFSP.

18 May 2000; accepted 24 July 2000

The Productive Conformation of Arachidonic Acid Bound to Prostaglandin Synthase

M. G. Malkowski,[1] S. L. Ginell,[2] W. L. Smith,[1] R. M. Garavito[1]*

Prostaglandin H synthase-1 and -2 (PGHS-1 and -2) catalyze the committed step in prostaglandin synthesis and are targets for nonsteroidal anti-inflammatory drugs (NSAIDs) like aspirin. We have determined the structure of PGHS-1 at 3 angstrom resolution with arachidonic acid (AA) bound in a chemically productive conformation. The fatty acid adopts an extended L-shaped conformation that positions the 13proS hydrogen of AA for abstraction by tyrosine-385, the likely radical donor. A space also exists for oxygen addition on the antarafacial surface of the carbon in the 11-position (C-11). While this conformation allows endoperoxide formation between C-11 and C-9, it also implies that a subsequent conformational rearrangement must occur to allow formation of the C-8/C-12 bond and to position C-15 for attack by a second molecule of oxygen.

PGHSs convert AA, O_2, and two electrons to prostaglandin H_2 (PGH_2) in the committed step in prostaglandin synthesis. PGHSs catalyze two semi-independent reactions (*1*, *2*)—a *bis* oxygenase [cyclooxygenase (COX)] reaction that uses AA and two O_2 molecules to form PGG_2 and a peroxidase (POX) reaction in which PGG_2 undergoes a two-electron re-

duction to PGH_2. Two isoforms of PGHS (PGHS-1 and -2) are found in most, if not all, mammalian tissues. PGHS-1 is constitutively expressed and is involved in prostaglandin biosynthesis in response to hormone stimulation. The resulting prostanoids interact with cell surface G protein (heterotrimeric GTP–binding protein)–linked receptors to mediate "housekeeping" functions, including the regulation of renal water and sodium metabolism, stomach acid secretion, parturition, and hemostasis. In contrast, PGHS-2 is an inducible enzyme that is expressed transiently in response to growth factors, tumor promoters, or cytokines. Prostanoids produced via PGHS-2 are involved in cell replication and differentiation. Both PGHS-1 and -2 are of pharmacological importance because they are targets for aspirin and NSAIDs. Aspirin inhibition of PGHS-1 lowers the risk for mortality from cardiovascular disease (*3*, *4*), whereas inhibition of PGHS-2 acts to reduce inflammation, fever, and pain (*5*–*7*); various cancers (*8*–*12*); and possibly Alzheimer's disease (*13*). The recently approved COX-2 inhibitors, which lack the gastrointestinal side effects associated with more classical NSAIDs (*14*, *15*), directly target PGHS-2.

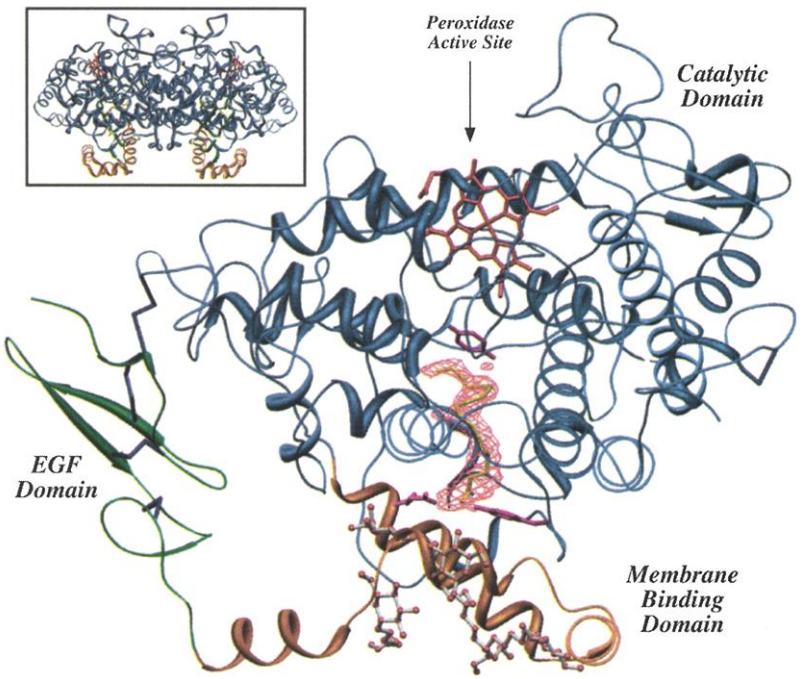

Fig. 1. A ribbon representation of the Co^{3+}-oPGHS-1 monomer with AA bound in the COX channel. The EGF domain, MBD, and catalytic domain are shown in green, orange, and blue, respectively; Co^{3+}-protoporphyrin IX is depicted in red, disulfide bonds (Cys^{36}-Cys^{47}, Cys^{37}-Cys^{159}, Cys^{41}-Cys^{57}, Cys^{59}-Cys^{69}, and Cys^{569}-Cys^{575}) in dark blue, and side chain atoms for COX channel residues Arg^{120}, Tyr^{355}, and Tyr^{385} in magenta. Also shown is a $F_o - F_c$ simulated annealing omit map contoured at 1.5σ for AA (yellow). The four β-OG detergent molecules (ball and stick) are shown bound to the MBD, including one detergent molecule found just below Arg^{120} and Tyr^{355} within the opening to the COX channel. (Inset) The native dimer with the twofold axis running vertical. All figures were created fully or in part using SETOR (*44*).

Table 1. Summary of data collection and refinement statistics.

Item	AA-1	AA-2
Spacegroup	$P6_522$	$P6_522$
a (Å)	182.10	182.05
b (Å)	182.10	182.05
c (Å)	103.64	103.14
Resolution (Å)	9.0 to 3.0	9.0 to 3.1
No. of unique reflections ($F > 0\sigma$)	19163	16954
Completeness (%)	93 (81)*	92 (81)*
R merge, all data (%; $I > 0\sigma$)†	6.7 (34.7)*	9.5 (34.1)*
No. of atoms in refinement	4780	4729
R factor (%; reflections $> 2\sigma$ on *F*)‡	21.6	22.4
Free-*R* factor (%; reflections $> 2\sigma$ on *F*)§	29.0	28.7
Mean positional error (Å)‖	0.38	0.40
RMSD in bond distance (Å)	0.009	0.010
RMSD in bond angle (°)	1.508	1.545
RMSD in improper angle (°)	1.035	1.081
RMSD in dihedral angle (°)	21.957	22.273

*Values in parenthesis represent values in last shell: AA-1 (3.1 to 3.0 Å) and AA-2 (3.2 to 3.1 Å). †*R* merge = $\Sigma|I - \langle I\rangle|/\Sigma I$, where *I* is the observed intensity of an individual reflection, and $\langle I\rangle$ is the mean intensity of that reflection. ‡*R* factor = $\Sigma|F_o - F_c|/\Sigma F_o$, where F_o and F_c are observed and calculated structure factors, respectively. §Free-*R* factor is the cross validation *R* factor computed for the test set of reflections (5% of the total were used), which are omitted during the refinement process. ‖Upper limit, calculated from 6.0 to 3.0 Å.

[1]Department of Biochemistry and Molecular Biology, Michigan State University, East Lansing, MI 48824–1319, USA. [2]Structural Biology Center, Argonne National Laboratory, Argonne, IL 60439, USA.

*To whom correspondence should be addressed. E-mail: garavito@magaera.bch.msu.edu

also well resolved. Bound AA was clearly observed in the initial $2F_o - F_c$ (F_o, observed structure factor; F_c, calculated structure factor) electron density maps. Iterative model building, with the use of standard $F_o - F_c$ difference electron density maps and simulated annealing omit maps followed by positional refinement, allowed the accurate placement of AA in the active site (Fig. 2) despite the limited resolution.

AA is bound within the COX active site and adopts an extended L-shaped conformation with two kinks in the center (Fig. 2). Carbons of AA C-1 through C-3 bind in the channel with the carboxylate positioned to interact with the guanidinium group of Arg^{120} and the phenolic oxygen of Tyr^{355}. C-7 through C-14 form an S shape that weaves the substrate around the side chain of Ser^{530}. C-13 is close to the phenolic oxygen of Tyr^{385} and is oriented properly for abstraction of the pro*S* hydrogen. The S shape also positions C-11 above a small pocket into which O_2 could presumably migrate from the lipid bilayer (Fig. 2A). Thus, C-11 would be accessible to O_2 from the side opposite (antarafacial) to hydrogen abstraction, a known aspect of the reaction (*26*). The ω-end of the substrate (C-14 through C-20) binds in a cul-de-sac along helices 6 (residues 325 through 353) and 17 (residues 520 through 535) between Ser^{530} and Gly^{533} (Fig. 2).

As expected, the residues lining the COX channel make multiple hydrophobic interactions with AA (Fig. 3). Of 49 interactions between the enzyme and substrate, only the two carboxylate interactions with Arg^{120} and Tyr^{355} are hydrophilic. Fatty acid–enzyme contacts can be divided into three spatial regions in terms of the substrate carbons: the apical end (C-1 through C-7), the "catalytic" core (C-8 through C-13), and the ω-end (C-14 through C-20). Some of the more interesting substrate-protein interactions are discussed below.

At the apical end, the carboxylate of AA forms an edge-on salt bridge with the guanidinium group of Arg^{120} (Fig. 2B). Arg^{120} lies at the base of the COX active center above the MBD, protruding into the COX channel. Earlier studies (*16*–*18*) predicted that the interaction of the AA carboxylate with Arg^{120} was a major determinant in substrate binding. Indeed, the mutation of Arg^{120} to glutamine increases the K_m (Michaelis constant) of oPGHS-1 for AA by 1000-fold, demonstrating how critical this ionic interaction is for substrate binding to PGHS-1 (*27*). In contrast, Arg^{120} in PGHS-2 is not critical for substrate binding (*28*), a result that cannot yet be adequately explained.

Tyr^{355} lies across from Arg^{120} at the base of the COX channel (Fig. 2) such that its hydroxyl group forms a hydrogen bond to the carboxylate of AA. This interaction appears important in the discrimination between the stereoisomers of certain NSAIDs and may also play a role in substrate binding (*27*). Leu^{531} is also in close proximity to Arg^{120}, and its Cδ1 methyl group abuts the carboxylate of AA (Fig. 2A). Mutating Leu^{531} to lysine inactivates the enzyme (*29*), most likely due to competition with Arg^{120} for the substrate's carboxylate. Similarly, the $Leu^{531} \rightarrow Asp^{531}$ (L531D) (*30*) and L531N mutations have native-like K_m values but only one-tenth of the native COX activity (*29*). Apparently, the introduction of hydrophilic residues at residue 531 can lead to stable but improper liganding of the substrate carboxylate to the enzyme. Thus, the proper AA binding to Arg^{120} is critical for enzyme activity in PGHS-1, and even modest structural changes in the immediate environment are not tolerated.

Above the carboxylate end of AA, the fatty acid chain runs along Ile^{523} and then bends over Val^{349}, Ala^{527}, and Ser^{530} (Fig. 2). Ile^{523} makes hydrophobic contacts with C-2 and the C-5/C-6 double bond (Fig. 3). Residue 523, which is a valine in PGHS-2, is the only residue in the first shell of COX active site residues that differs between PGHS-1 and PGHS-2. Having a valine at this position in PGHS-2 increases the size of the COX channel, a feature that is exploited by PGHS-2–specific NSAIDs (*31*) and may account for some isozyme differences in substrate utilization (*32*). However, the Cγ2 atom of Ile^{523} abuts the substrate, a contact that could also be present with Val^{523} in PGHS-2. The I523V (*30*) mutation in PGHS-1 decreases the COX activity by 30% (*33*), a result that demonstrates that subtle—and perhaps more global—differences exist between nearly identical active sites in the two isozymes.

Residues in the catalytic core region surround the center of the substrate (C-8 to C-13) and the radical donor/acceptor Tyr^{385}. These residues can be divided into classes:

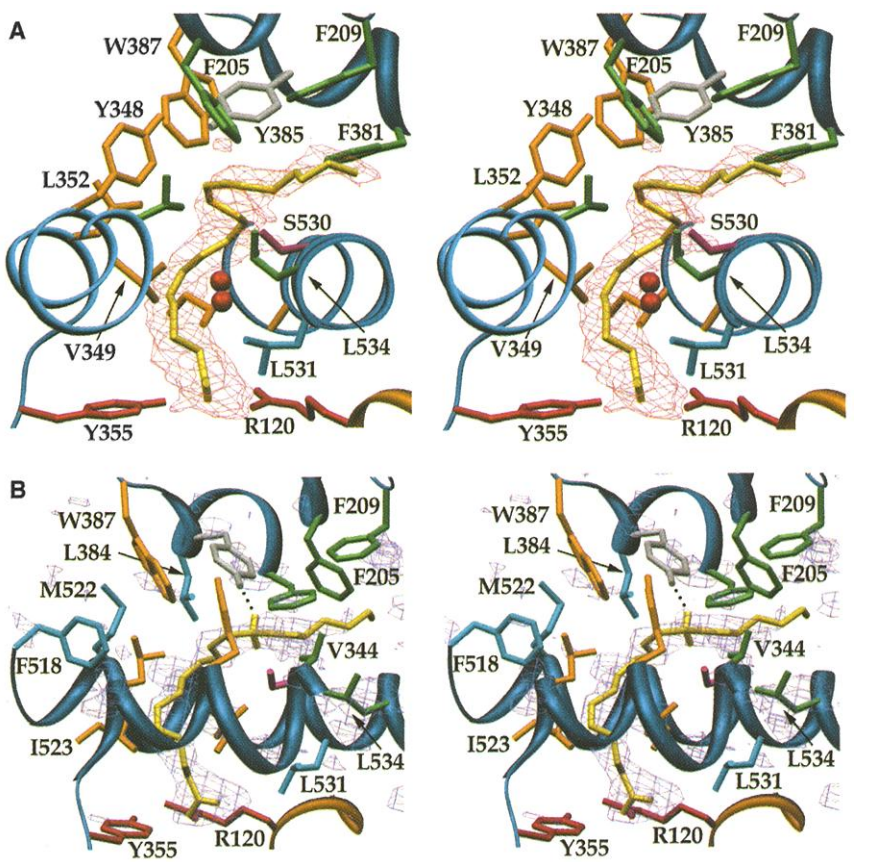

Fig. 2. AA bound in the COX channel (*30*). (**A**) Stereo view of AA bound in the COX channel. The $F_o - F_c$ simulated annealing omit electron density contoured at 1.5σ for AA (yellow) is shown. Side chain atoms for all residues that contact the substrate at the carboxylate, C-2 through C-11, and C-14 through C-20 are colored red, orange, and green, respectively. Ser^{530} (magenta), which is acetylated by aspirin, lies below Tyr^{385} (gray), the likely radical donor during catalysis. Leu^{531} (light blue) lies above Arg^{120} but does not contact the substrate. The two red spheres represent the presumed location of O_2 for attack on C-11. (**B**) The view of the COX active site rotated 90° about the vertical axis [using the same color scheme as in (A)]. The $F_o - F_c$ difference density (purple) around the COX molecule is contoured at 2.5σ; the largest peak in the map constitutes that for AA. Residues Phe^{518}, Leu^{384}, and Met^{522} (in light blue) along with Phe^{381} and Trp^{387} constitute the endoperoxide pocket. Hydrogen atoms for C-13 have been modeled. The 13pro*S* hydrogen is 2.3 Å from the OH group of Tyr^{385}.

those that come within 4 Å of the substrate (Tyr[348], Leu[352], Trp[387], and Ser[530]) and those that do not (Leu[384], Phe[518], and Met[522]). Ser[530], which is acetylated by aspirin treatment, abuts against the substrate (Fig. 2A); its C_α and C_β atoms make hydrophobic contacts with C-10 and C-16, while the Oγ atom lies underneath C-13. When Ser[530] is replaced with alanine, the enzyme retains 60 to 80% of its native COX activity without changing the K_m for AA (*34*). Thus, the serine hydroxyl is neither essential for catalysis nor for AA binding. A S530T (*30*) mutation reduces the COX activity to 15% that of native enzyme, with a sixfold increase in K_m (*29*, *34*). Modeling an extra methyl group at this position suggests that the mutation affects the conformation of the neighboring residues (Gly[526], Ala[527], and Leu[534]), which contact both the carboxyl and ω ends of the substrate.

Phe[381], Leu[384], Trp[387], Phe[518], and Met[522] form a pocket that could accommodate the conformational transitions involving C-8 through C-12 during O_2 addition and endoperoxide ring formation (Fig. 2B). Of these residues, Leu[384], Phe[518], and Met[522] do not contact the substrate, whereas Trp[387] contacts both the substrate and Tyr[385], the putative radical donor. C-11, the first site of attack by O_2, and C-12 abut against the ring edge of Trp[387]. The recently constructed W387F and W387L (*30*) mutants (*33*) produce considerable amounts of 11(*R*)-hydroperoxyeicosatetraenoic (11*R*-HETE), presumably arising from the failure to form the endoperoxide bridge. Thus, Trp[387] may help properly align or stabilize intermediates during PGG_2 formation.

Positioned below Tyr[385], the phenolic group of Tyr[348] hydrogen bonds to the phenolic group of Tyr[385], an interaction seen in all other PGHS-1 crystal structures (*16*–*18*). A Y348F (*30*) mutation has no effect on COX activity (*35*), indicating that the conserved hydrogen bond between the hydroxyl groups of Tyr[348] and Tyr[385] is not important for catalysis. However, Tyr[348] makes three hydrophobic contacts with carbons 12 through 14 of the substrate (Fig. 3) and may help position C-13 for hydrogen abstraction.

The ω-end of AA lies between helices 6 and 17 such that Phe[205], Phe[209], Leu[344], Phe[381], and Leu[534] form a hydrophobic cage around the last six carbons of the substrate (Figs. 2 and 3). At C-17, the end of AA turns abruptly, placing C-20 against Gly[533]. The G533A (*30*) mutant in PGHS-1 has no COX activity (*29*), suggesting that a clash between methyl group of alanine and C-20 is enough to prevent the proper binding of AA. The hypothesis that the more spacious COX active site in PGHS-2 affords added variability in substrate binding (*20*, *32*, *36*) is supported by the fact that the G533A (*30*) mutant in PGHS-2 retains some COX activity (*37*). Only when Gly[533] in PGHS-2 was mutated to a leucine or valine was all COX activity lost (*37*). The larger COX active site in PGHS-2 is also used to explain why aspirin acetylation inactivates COX activity in PGHS-1 but allows turnover of AA to 15*R*-HETE in PGHS-2 (*38*). The recent work by Rowlinson *et al.* (*37*) shows how the mutation of Gly[533] in PGHS-2 alters the enzyme's activity toward 18 carbon unsaturated fatty acids, suggesting that the shape and size of this binding region may be important in determining substrate selectivity.

The observed structure of AA bound in the COX active site agrees well, on a qualitative level, with the productive conformations of AA proposed by a recent modeling study (*37*) and a crystal structure of mouse PGHS-2 containing a mixture of product and substrate (*21*). It also places considerable constraints on any proposed mechanism for enzyme catalysis. However, it

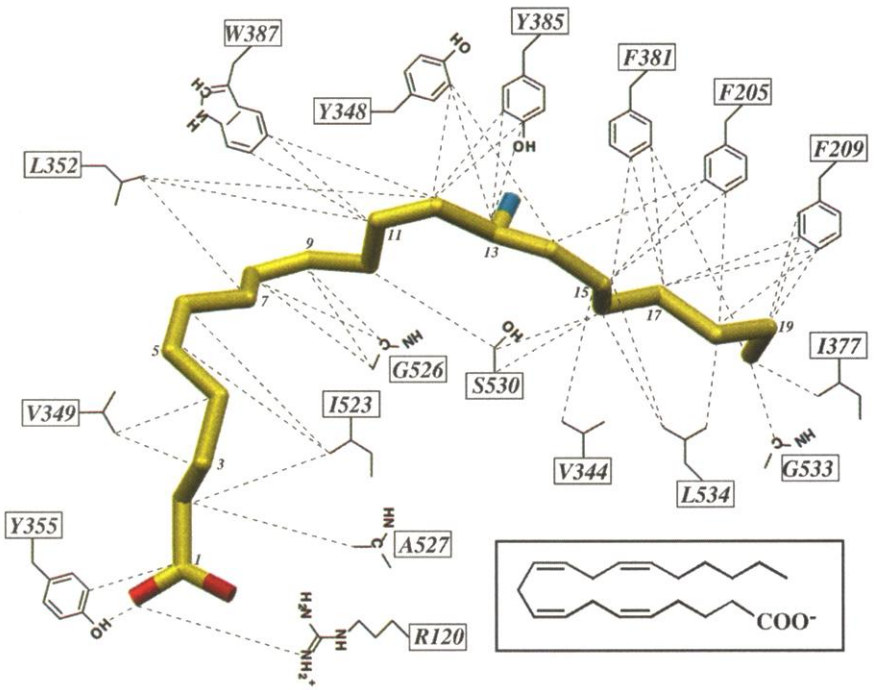

Fig. 3. A schematic of interactions between AA and COX channel residues (*30*). Carbon atoms of AA are yellow, oxygen atoms red, and the 13pro*S* hydrogen blue. All dashed lines represent interactions within 4.0 Å between the specific side chain atom of the protein and AA; the structures AA-1 and AA-2 revealed the same set of 49 contacts. Only two of these contacts between AA and the COX channel residues are hydrophilic. The carboxylate forms a salt bridge to the guanidinium atom of Arg[120] (distance = 2.4 Å; angle = 143°) and a hydrogen bond to the OH group of Tyr[355] (distance = 3.1 Å; angle = 115°). (Inset) A schematic of the chemical structure of AA.

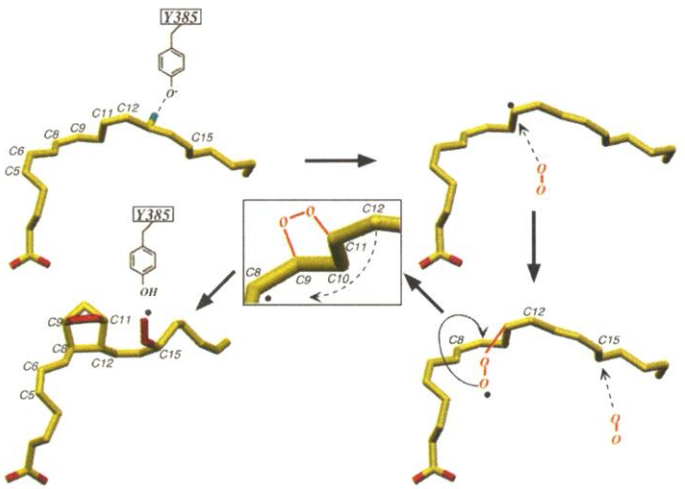

Fig. 4. Mechanistic sequence for converting AA to PGG_2 (*30*). Abstraction of the 13-pro*S* hydrogen by the tyrosyl radical leads to the migration of the radical to C-11 on AA. Attack of molecular oxygen, coming from the base of the COX channel, occurs on the side antarafacial to hydrogen abstraction. As the 11*R*-peroxyl radical swings over C-8 for an *R*-side attack on C-9 to form the endoperoxide bridge, C-12 is brought closer to C-8 via rotation about the C-10/C-11 bond allowing the formation of the cyclopentane ring. The movement of C-12 also positions C-15 optimally for addition of a second molecule of oxygen, formation of PGG_2, and the migration of the radical back to Tyr[385].

must be noted that PGHS-1 and -2 do not convert AA to PGG_2 with 100% efficiency (*26*). The PGHS isoforms make low levels of 11*R*-HETE and 15(*R/S*)-hydroperoxyeicosatetraenoic acids (15-HETE) due to the existence of minor alternate conformers of AA within the COX active site (*26*). Accordingly, the observed electron density for AA in oPGHS-1 may be an average of more than one AA conformer. Nonetheless, the modeled conformation of AA satisfies the stereochemical requirements of the initial catalytic steps, allowing a structurally valid sequence of catalytic events for the COX reaction to be envisioned (Fig. 4).

AA is positioned such that a Tyr^{385} phenolic radical can abstract the 13pro*S* hydrogen (Fig. 2B). Oxygen then migrates into a small pocket (Val^{349}, Ala^{527}, Ser^{530}, and Leu^{531}) (Fig. 2A) below C-11 and attacks the substrate from the side antarafacial to that of hydrogen abstraction to yield an 11*R*-peroxyl radical intermediate (*26*). The 11*R*-peroxyl radical then attacks C-9 to produce the endoperoxide bridge, which produces a radical centered on C-8 (Fig. 4). However, the extended conformation of AA cannot permit facile ring closure between C-12 and C-8 at this stage of the reaction because the distance between C-8 and C-12 is about 5 Å. Thus, a major reconfiguration of the substrate must occur concomitant with or immediately following formation of the endoperoxide bridge.

We propose that the conformational transition involves substantial movement of the ω-end of AA toward the apical half of the molecule. The loss of the C-11/C-12 double bond with the formation of the 11*R*-peroxyl moiety increases the local conformational freedom for the attack on C-9. The peroxyl could then swing "over" C-8 for a *R*-side attack on C-9 (Fig. 4), bringing C-12 closer to C-8 via rotation about the C-10/C-11 bond. This conformational transition would also reposition atoms C-13 to C-20. A *S*-side attack on C-9 is less likely due to steric hindrance from C-7. Formation of the endoperoxide bridge also results in the loss of the C-8/C-9 double bond, which again increases local conformational freedom. The radical, now on C-8, is ready for attack on C-12 (Fig. 4). Additionally, these conformational transitions in the substrate could also position C-15 optimally for the addition of the second O_2 molecule and for hydrogen donation by Tyr^{385} to the 15*S*-peroxyl radical. The latter event completes the COX reaction and returns the radical to the catalytic tyrosine for the next turnover.

Further mutagenic and structural studies of oPGHS-1 interactions with fatty acids are needed to confirm the catalytic events proposed here. The functional differences between PGHS-1 and PGHS-2 in response to identical mutations (e.g., R120Q and G533A) (*30*) also remain unexplained, but suggest that the two isoforms have subtle but distinct differences in active site structures, which remain to be elucidated.

References and Notes

1. L. J. Marnett *et al.*, *J. Biol. Chem.* **274**, 22903 (1999).
2. W. L. Smith, D. L. DeWitt, R. M. Garavito, *Annu. Rev. Biochem.* **69**, 149 (2000).
3. P. Patrignani *et al.*, *J. Pharmacol. Exp. Ther.* **271**, 1705 (1994).
4. C. Patrono, *N. Engl. J. Med.* **330**, 1287 (1994).
5. D. Riendeau *et al.*, *Br. J. Pharmacol.* **121**, 105 (1997).
6. C. J. Smith *et al.*, *Proc. Natl. Acad. Sci. U.S.A.* **95**, 13313 (1998).
7. Y. Zhang *et al.*, *J. Pharmacol. Exp. Ther.* **283**, 1069 (1997).
8. H. Sheng *et al.*, *J. Clin. Invest.* **99**, 2254 (1997).
9. G. N. Levy, *FASEB J.* **11**, 234 (1997).
10. S. L. Kargman *et al.*, *Cancer Res.* **55**, 2556 (1995).
11. W. Kutchera *et al.*, *Proc. Natl. Acad. Sci. U.S.A.* **93**, 4816 (1996).
12. D. Hwang, D. Scollard, J. Byrne, E. Levine, *J. Natl. Cancer Inst.* **90**, 455 (1998).
13. P. L. McGeer and E. G. McGeer, *J. Leukoc. Biol.* **65**, 409 (1999).
14. L. J. Marnett and A. S. Kalgutkar, *Curr. Opin. Chem. Biol.* **2**, 482 (1997).
15. D. L. DeWitt, *Mol. Pharmacol.* **4**, 625 (1999).
16. D. Picot, P. J. Loll, R. M. Garavito, *Nature* **367**, 243 (1994).
17. P. J. Loll, D. Picot, R. M. Garavito, *Nature Struct. Biol.* **2**, 637 (1995).
18. P. J. Loll, D. Picot, O. Ekabo, R. M. Garavito, *Biochemistry* **35**, 7330 (1996).
19. R. G. Kurumbail *et al.*, *Nature* **384**, 644 (1996).
20. C. Luong *et al.*, *Nature Struct. Biol.* **3**, 927 (1996).
21. J. R. Kiefer *et al.*, *Nature* **405**, 97 (2000).
22. W. L. Smith *et al.*, *Biochemistry* **31**, 3 (1992).
23. M. G. Malkowski, M. J. Theisen, A. Scharmen, R. M. Garavito, *Arch. Biochem. Biophys.* **380**, 39 (2000).
24. Crystals of Co^{3+}-oPGHS-1 complexed with AA were prepared as described in (*23*). Briefly, crystals were grown in sitting-drops by combining the Co^{3+}-oPGHS-1:AA complex with buffer composed of the following: 0.64 M sodium citrate, 0.3 to 0.6 M LiCl, 1 mM NaN_3, 0.33% (w/v) n-octyl-β-D-glucopyranoside (β-OG), at pH 6.5. The buffer was equilibrated over reservoir solutions composed of the following: 0.64 to 0.84 M sodium citrate, 0.3 to 0.6 M LiCl, and 1 mM NaN_3 at 20°C. The crystals were harvested and transferred into stabilization buffer (0.9 M sodium citrate, pH 6.5, 1.0 M LiCl, 0.15% (w/v) β-OG), followed by a single-step transfer into stabilization buffer with 24% (w/v) sucrose as a cryoprotectant. The crystals were immediately frozen in liquid propane at −165°C. Data were collected on beamline 19-ID of the Structural Biology Center (Advanced Photon Source, Argonne, IL) and were processed using HKL2000 (*39*). The structure of the first Co^{3+}-oPGHS-1:AA complex (AA-1) was solved by molecular replacement using CNS version 0.9a (*40*), and the protein portion of the refined oPGHS-1/flurbiprofen complex (Protein Data Base entry 1CQE) as the search model. The top 10 peaks identified by the rotation search were optimized using Patterson Correlation refinement; subsequent translation searches confirmed the space group as $P6_522$. Initial rigid-body refinement, employing the maximum likelihood target using amplitudes, a bulk solvent correction, and an overall temperature (*B*) factor correction, resulted in initial *R* and free-*R* values of 31.4% and 30.2%, respectively. After positional and group *B*-factor refinement, analysis of $2F_o - F_c$ electron density maps (contoured at 1.2σ) allowed the placement of nine carbohydrate residues, Co^{3+}-protoporphyrin IX, four β-OG detergent molecules, and AA in the COX channel. The electron density for the carboxylate moiety and carbons C-2 to C-17 of AA was always strong; weaker electron density was always seen for C-18 to C-20 (Fig. 2). The final model, containing 109 water molecules, has *R* and free-*R* values of 21.6% and 29.0%, respectively (*41*). All residues lie within the most favored or allowed regions of the Ramachandran plot, and the parameters evaluated by PROCHECK (*42*) are well within the bounds established from well-refined structures at equivalent resolution. The AA-2 data set was refined independently using the same protocols employed for the AA-1 dataset. The final model has *R* and free-*R* values of 22.4% and 28.7%, respectively, and contains nine carbohydrate residues, Co^{3+}-protoporphyrin IX, and AA bound in the COX channel. However, unlike AA-1, only 81 water molecules, two β-OG detergent molecules, and two detergent head groups could be fit. The structures of AA-1 and AA-2 are virtually identical with a root mean square deviation (RMSD) between 550 (out of 554) Cα atoms of 0.17 Å. Furthermore, the RMSD between the 22 atoms of AA bound in each structure is 0.34 Å, well within the experimental error of both structures (Table 1).
25. As described in detail by R. M. Garavito, D. Picot, and P. J. Loll (*43*), oPGHS-1 crystals are very sensitive to manipulation for data collection, most likely due to their sensitivity to changes in the detergent environment. Thus, the $P6_522$ crystals vary markedly in x-ray diffraction quality (i.e., mosaicity, disorder, and diffraction limit) and only 1 in 10 crystals diffract well enough for data collection to beyond 3.5 Å resolution. Hence, the two best data sets (AA-1 and AA-2) out of 10 were chosen for structure determination to 3.0 Å, were refined independently, and then were compared in order to detect artifacts arising from the effects of crystal manipulation on diffraction.
26. E. D. Thuresson, K. M. Lakkides, W. L. Smith, *J. Biol. Chem.* **275**, 8501 (2000).
27. D. P. Bhattacharyya *et al.*, *J. Biol. Chem.* **271**, 2179 (1996).
28. C. J. Rieke, A. M. Mulichak, R. M. Garavito, W. L. Smith, *J. Biol. Chem.* **274**, 17109 (1999).
29. T. Shimokawa and W. L. Smith, *J. Biol. Chem.* **267**, 12387 (1992).
30. Single-letter abbreviations for the amino acid residues are as follows: A, Ala; C, Cys; D, Asp; E, Glu; F, Phe; G, Gly; H, His; I, Ile; K, Lys; L, Leu; M, Met; N, Asn; P, Pro; Q, Gln; R, Arg; S, Ser; T, Thr; V, Val; W, Trp; and Y, Tyr.
31. J. K. Gierse *et al.*, *J. Biol. Chem.* **271**, 15810 (1996).
32. O. Laneuville, *et al.*, *J. Biol. Chem.* **270**, 19330 (1995).
33. W. L. Smith, unpublished data.
34. D. L. DeWitt *et al.*, *J. Biol. Chem.* **265**, 5192 (1990).
35. L. C. Hsi *et al.*, *Biochem. Biophys. Res. Commun.* **207**, 652 (1995).
36. O. Laneuville *et al.*, *J. Pharmacol. Exp. Ther.* **271**, 927 (1994).
37. S. W. Rowlinson, B. C. Crews, C. A. Lanzo, L. J. Marnett, *J. Biol. Chem.* **274**, 23305 (1999).
38. M. Lecomte *et al.*, *J. Biol. Chem.* **269**, 13207 (1994).
39. Z. Otwinowski and W. Minor, in *Methods in Enzymology: Macromolecular Crystallography, Part A*, C. W. Carter and R. M. Sweet, Eds. (Academic Press, San Diego, 1997), vol. 276, pp. 307.
40. A. T. Brünger *et al.*, *Acta Crystallogr. D* **54**, 905 (1998).
41. The following side chains have been truncated to Ala due to poor side chain density: Arg^{79}, Arg^{83}, Lys^{169}, Gln^{170}, Asp^{173}, Glu^{175}, Lys^{186}, Lys^{215}, Lys^{248}, Glu^{267}, Glu^{290}, Lys^{317}, Arg^{396}, Gln^{400}, Glu^{405}, Asp^{416}, Lys^{473}, Gln^{479}, Lys^{485}, and Glu^{486}.
42. R. A. Laskowski, M. W. MacArthur, D. S. Moss, J. M. Thornton, *J. Appl. Crystallogr.* **26**, 283 (1993).
43. R. M. Garavito, D. Picot, P. J. Loll, *J. Bioenerg. Biomembr.* **28**, 13 (1995).
44. S. V. Evans, *J. Mol. Graphics* **11**, 134 (1993).

45. Supported by NIH grants PO1 GM57323 (W.L.S. and R.M.G.) and R01 HL56773 (R.M.G.). M.G.M. was supported by NIH National Research Service Award F32 HL10170-01. Use of the Advanced Photon Source was supported by the U.S. Department of Energy, Basic Energy Sciences, Office of Energy Research, under contract no. W-31-109-Eng-38. Coordinates have been deposited at the Protein Data Bank (entry code 1DIY).

17 February 2000; accepted 30 June 2000